

# Planck priors for dark energy surveys

Pia Mukherjee,<sup>1</sup> Martin Kunz,<sup>2</sup> David Parkinson,<sup>1</sup> and Yun Wang<sup>3</sup>

<sup>1</sup>*Astronomy Centre, University of Sussex, Brighton BN1 9QH, United Kingdom*

<sup>2</sup>*Astronomy Centre, University of Sussex, Brighton BN1 9QH,*

*United Kingdom; Department of Theoretical Physics,*

*Univ. of Geneva, 24 Quai E. Ansermet, 1211 Geneve 4, Switzerland*

<sup>3</sup>*Homer L. Dodge Department of Physics & Astronomy,*

*Univ. of Oklahoma, 440 W Brooks St., Norman, OK, USA*

(Dated: October 26, 2018)

Although cosmic microwave background (CMB) anisotropy data alone cannot constrain simultaneously the spatial curvature and the equation of state of dark energy, CMB data provide a valuable addition to other experimental results. However computing a full CMB power spectrum with a Boltzmann code is quite slow; for instance if we want to work with many dark energy and/or modified gravity models, or would like to optimize experiments where many different configurations need to be tested, it is possible to adopt a quicker and more efficient approach.

In this paper we consider the compression of the projected Planck CMB data into four parameters,  $R$  (scaled distance to last scattering surface),  $l_a$  (angular scale of sound horizon at last scattering),  $\Omega_b h^2$  (baryon density fraction) and  $n_s$  (powerlaw index of primordial matter power spectrum), all of which can be computed quickly. We show that, although this compression loses information compared to the full likelihood, such information loss becomes negligible when more data is added. We also demonstrate that the method can be used for scalar field dark energy independently of the parametrisation of the equation of state, and discuss how this method should be used for other kinds of dark energy models.

PACS numbers: 98.80.Es, 98.80.-k, 98.80.Jk

## I. INTRODUCTION

Dark energy model building continues to be an active area of research [1, 2, 3, 4, 5, 6, 7, 8, 9, 10]. While current data remain consistent with a cosmological constant explanation for dark energy, other possibilities are not yet ruled out, especially if theoretical motivation can be found to tighten their predictions about the data [11]. New theoretical ideas thus may bolster support in favour of an exotic component of matter or a modification of gravity beyond some length scale.

On the observational front, recognizing the need for better data, many future dark energy surveys have been proposed, classified by the Dark Energy Task Force as stage III and stage IV experiments [12]. The realisable constraints from these surveys depend sensitively on the external or prior information that will be available in the future. A crucial external data set will come from the Planck satellite, which will place strong constraints on a range of cosmological parameters. It is therefore important to include this data for forecasts and optimisations of instrument performance for the stage III and IV dark energy surveys. This in turn requires a rapid way to evaluate the predicted Planck likelihood, preferably without the necessity to run a Boltzmann code.

Some of us have shown that the information from the WMAP CMB experiment [13] can be effectively and simply incorporated into a likelihood analysis of Type Ia supernovae (SN Ia) and baryon acoustic oscillation (BAO) data by including in the likelihood a term involving WMAP constraints on the CMB shift param-

eter ( $R$ ), the angular scale of the sound horizon at last scattering ( $l_a$ ), and the baryon density  $\Omega_b h^2$ , in Gaussian form together with their full covariance matrix [14]. The idea being that the calculation of full CMB spectra at each parameter point can be avoided, so that a Markov Chain Monte Carlo (MCMC) analysis proceeds very quickly. The merit lies in the method being independent of the dark energy model used as long as only background (or homogeneous) quantities are varied.

In this paper we extend the method to projected Planck data, which is significantly more accurate than WMAP data. We derive and test this simple prescription, compare it to a full likelihood analysis of simulated Planck data, and conclude that when such a Planck prior is combined with future dark energy surveys useful complementary information from the CMB is retained and there is no significant information loss. Hence the prescription remains an effective way to incorporate constraints from Planck (or Planck priors) in the analyses of data from future dark energy surveys.

## II. COMPONENTS OF THE PROPOSED PLANCK LIKELIHOOD

Let us first introduce the parameters that we are proposing to use as an effective summary of the information contained in a CMB spectrum:

$$R \equiv \sqrt{\Omega_m H_0^2} r(z_{CMB}), \quad l_a \equiv \pi r(z_{CMB}) / r_s(z_{CMB}), \quad (1)$$

where  $r(z)$  is the comoving distance from the observer to redshift  $z$ , and  $r_s(z_{CMB})$  is the comoving size of the sound-horizon at decoupling. We give the details of the formulae used in appendix A.

In this scheme,  $l_a$  describes the peak location through the angular diameter distance to decoupling and the size of the sound horizon at that time. If the geometry changes, either due to non-zero curvature or due to a different equation of state of dark energy,  $l_a$  changes in the same way as the peak structure.  $R$  encodes similar information, but in addition contains the matter density which is connected with the peak height. In a given class of models (for example, quintessence dark energy), these parameters are “observables” relating to the shape of the observed CMB spectrum, and constraints on them remain the same independent of (the prescription for) the equation of state of the dark energy. Furthermore,  $R$  and  $l_a$  are very well constrained by WMAP and even better by Planck and their likelihoods are almost perfectly Gaussian (remaining so under different treatments of dark energy), so that a Gaussian likelihood term together with the corresponding covariance matrix retains almost all of the information on these derived parameters. With curvature held fixed, an even simpler set up using just  $R$  sufficed and has been used by many authors, including [15, 16].

As a caveat we note that if some assumptions regarding the evolution of perturbations are changed, then the corresponding  $R$  and  $l_a$  constraints and covariance matrix will need to be recalculated under each such hypothesis, for instance if massive neutrinos were to be included, or even if tensors were included in the analysis [28]. Further  $R$  as defined in Eq. (1) can be badly constrained and quite useless if the dark energy clusters as well, e.g. if it has a low sound speed, as in the model discussed in [30]. However, as discussed further below we checked that our constraints are valid at least for scalar-field dark energy models, independent of the parametrisation of  $w(z)$ .

In addition to  $R$  and  $l_a$  we use the baryon density  $\Omega_b h^2$ , and optionally the spectral index of the scalar perturbations  $n_s$ , as these are strongly correlated with  $R$  and  $l_a$ , which means that we will lose information if we do not include these correlations.

### III. SIMULATED DATA

Our simulation and treatment of Planck data is as in [17]. We include the temperature and polarization (TT, TE, and EE) spectra from three temperature channels with specification similar to the HFI channels of frequency 100 GHz, 143 GHz, and 217 GHz, and one 143 GHz polarization channel, following the current Planck documentation,<sup>1</sup>. The full likelihood is constructed as-

suming a sky coverage of 0.8. We choose a fiducial model close to the WMAP best fit LCDM model:  $\Omega_b h^2 = 0.022$ ,  $\Omega_m h^2 = 0.127$ ,  $h = 0.73$ ,  $\Omega_k = 0$ ,  $w_0 = -1$ , and  $w_a = 0$ .

For the Baryon Acoustic Oscillation part, we use the experimental configuration outlined in the DETF report [12]. A Stage III spectroscopic experiment would cover 2000 square degrees with a redshift range of  $0.5 < z < 1.3$ , divided into 4 equally sized redshift bins, plus 300 square degrees with  $2.3 < z < 3.3$ . The experiment would obtain the spectra of  $10^7$  galaxies. This survey will measure the oscillations in the galaxy power spectrum, in the tangential direction (measuring  $r(z)$ ), and the radial direction (measuring  $dr(z)/dz = c/H(z)$ , providing a direct measurement of the Hubble parameter). To estimate the accuracy with which the radial and tangential oscillations can be measured, we apply these survey parameters to the fitting formulae described in [18]. These fitting formula only consider the accuracy with which the oscillations themselves can be measured, returning no information about the accuracy of the power spectrum measurement (as is done in e.g. [19, 20]). This is because the number of possible parameters contributing to the nature of the matter power spectrum, such as running of the spectral index, massive neutrinos, and non-linear bias, make this calculation very assumption dependent. In contrast, the positions of the oscillations is very robust with regard to these extra considerations.

For the Supernovae, we use a Stage III spectroscopic survey as described in the DETF report [12]. We assume a scaled-up version of the SNLS survey with 2000 supernovae in the range  $0.1 < z < 1$ , with a further 500 supernovae at low redshift. The dispersion in observed magnitude is the sum in quadrature of a fixed  $\sigma_D = 0.12$  with a second piece  $\sigma_m$ , which is fixed at 0.02 up to  $z = 0.4$  but then increases up to 0.03 by  $z = 1$ .

### IV. ANALYSIS

The full set of constraints on all parameters including  $R$  and  $l_a$  are determined through an MCMC based likelihood analysis [21] of simulated Planck data. Planck will provide much tighter constraints on parameters, and its posterior will be significantly better localized in parameter space than that of WMAP. The shape of the posterior (i.e. parameter correlations) is also found to be quite different from WMAP’s (further justifying the exercise of determining the best way to incorporate constraints from Planck separately from WMAP). While  $R$  and  $l_a$  were almost uncorrelated for WMAP data, this is no longer the case for Planck. Tables 1 and 2 show the estimated values and the covariance matrix for  $R$ ,  $l_a$ ,  $\Omega_b h^2$  and  $n_s$ . We have included  $n_s$  here because it is found to have a correlation with  $R$  and  $l_a$  and a different consideration of BAO data in the future, utilising the full shape of the matter power spectrum, might require the inclusion of  $n_s$  as a parameter. In the analysis presented in this paper, given the conservative treatment

<sup>1</sup> [www.rssd.esa.int/index.php?project=PLANCK&page=perf\\_top](http://www.rssd.esa.int/index.php?project=PLANCK&page=perf_top)

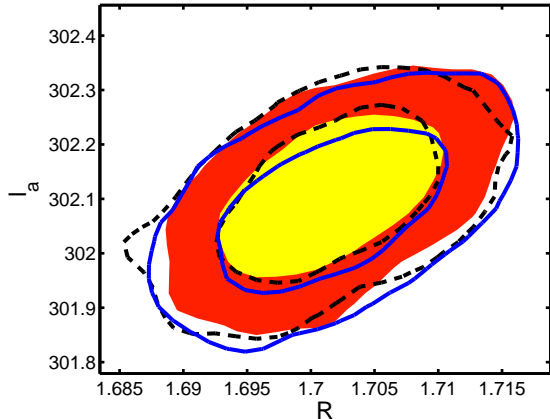


FIG. 1: This figure shows the projected 68% and 95% Planck constraints on  $R$  and  $l_a$  obtained assuming that dark energy were due to a cosmological constant (flat  $\Lambda$ CDM, dashed contours), a  $w_0, w_a$  model (shaded contours) and a kink model (solid contours), as described in the text.

of the BAO signal, the inclusion of  $n_s$  does not have a noticeable impact.

The first point to consider and re-test with Planck data is whether the constraints on  $R$ ,  $l_a$ ,  $\Omega_b h^2$  and  $n_s$ , and their corresponding covariance matrix are independent of the dark energy prescription used. In [14] we tested this for WMAP data for a cosmological constant, constant  $w$  and  $w_0-w_a$  models of dark energy, with and without curvature. Here we test it again for a flat model with a cosmological constant, and the  $w_0, w_a$  model and the kink model for dark energy, both with curvature, and for Planck quality data. In the  $w_0, w_a$  model  $w_X(z) = w_0 + w_a(1-a)$  [24] which corresponds to  $X(z) = a^{-3(1+w_0+w_a)} e^{3w_a(a-1)}$ . In the kink model the equation of state parameter  $w_X$  is described by its value today,  $w_0$ , its asymptotic value at high redshift,  $w_m$ , as well by two more parameters giving the location and speed of the transition from  $w_m$  to  $w_0$  [25]. In this case the energy density is derived through a numerical integration of the continuity equation. We found that there is no significant difference in the constraints on  $R$ ,  $l_a$ ,  $\Omega_b h^2$  and  $n_s$  obtained using these different models. See Figure 1.

Let us now test for the amount of information on parameters relevant to dark energy that is lost by considering a likelihood based on  $R$ ,  $l_a$ ,  $\Omega_b h^2$  and  $n_s$  rather than the full CMB spectra. Figure 2 shows  $w_0, w_a$  contours obtained from a full likelihood analysis of Planck simulated data (shaded contours) against contours reconstructed from the  $R$ ,  $l_a$ ,  $\Omega_b h^2$  and  $n_s$  likelihood (solid curves). We find that even in this limited 2D view there is significant information loss: The shaded contours from the full likelihood cover significantly less area than the open contours from the simpler likelihood. Due to the strong degeneracies which leave Planck basically unable to con-

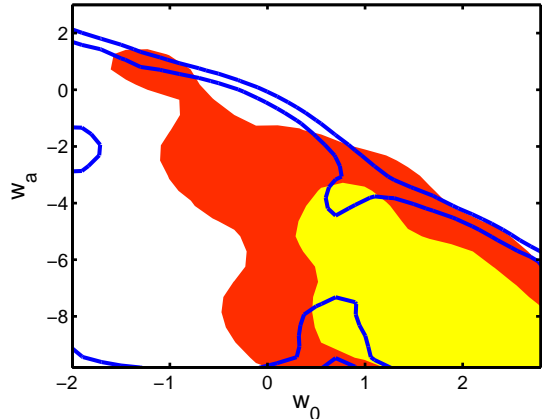


FIG. 2: This figure shows the Planck projected constraints on  $w_0, w_a$  obtained using a full likelihood analysis of simulated Planck data (shaded contours) and a simpler and quicker likelihood analysis based on  $R$ ,  $l_a$ ,  $\Omega_b h^2$  and  $n_s$  (solid contours). Information is thus lost by the simplified analysis.

strain cosmological parameters relating to dark energy and curvature on its own, the resulting contours depend strongly on the priors used.

It may be useful to note that given the  $R$ ,  $l_a$ ,  $\Omega_b h^2$  and  $n_s$  likelihood, one can implement a full likelihood analysis under different dark energy models more efficiently using Hamiltonian Monte Carlo. In this method the  $R$ ,  $l_a$ ,  $\Omega_b h^2$  and  $n_s$  likelihood is used as a guide to or an approximation of the true likelihood surface, but at each accepted point the likelihood is weighted using the full CMB spectra. We discuss this procedure in more detail in appendix C.

However the question remains, whether there is still an information loss when using the  $R$ ,  $l_a$ ,  $\Omega_b h^2$  and  $n_s$  likelihood from Planck when analysing SN Ia and/or BAO data, as compared to the full Boltzmann analysis of Planck data, which is much more time consuming and so limits our ability to consider many varied dark energy models. To address this we compared the outputs from two analyses. Firstly we performed a full MCMC run, i.e. including the full Planck likelihood and likelihoods from simulated stage III SN Ia and BAO surveys. Secondly we performed a MCMC analysis using the  $R$ ,  $l_a$ ,  $\Omega_b h^2$  and  $n_s$  likelihood from Planck together with the SN Ia and BAO likelihood. Fig. 3 shows the constraints obtained in each case. We conclude that there is effectively no information loss in using the  $R$ ,  $l_a$ ,  $\Omega_b h^2$  and  $n_s$  likelihood, in conjunction with the likelihood from a better SN Ia and/or BAO experiment, and this condensed data analysis proceeds much faster than an analysis involving the full CMB likelihood.

Another way to include a Planck prior in forecasting constraints from a future dark energy experiment is to do it via a Planck Fisher matrix. Consider the above likelihood analysis in comparison to a Fisher matrix treat-

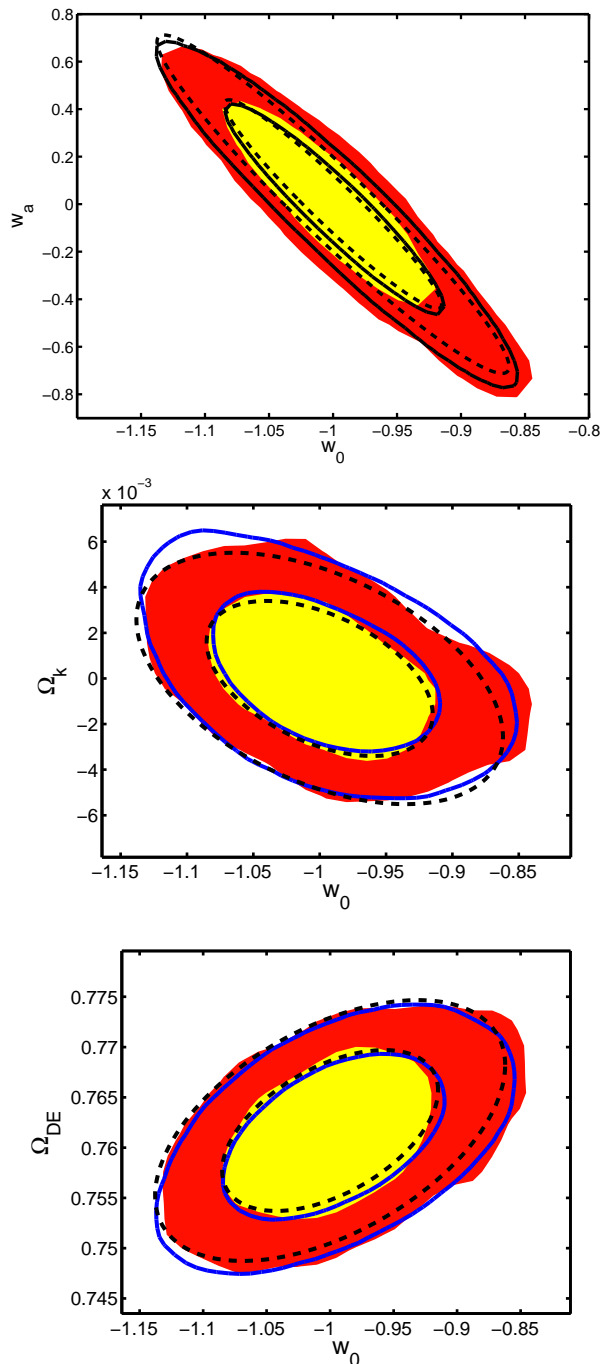


FIG. 3: This figure shows 2D confidence contours obtained using a full likelihood analysis of simulated Planck data in conjunction with stage III SN Ia and BAO data (shaded contours), contours obtained using the simplified  $R$ ,  $l_a$ ,  $\Omega_b h^2$  and  $n_s$  based likelihood analysis of Planck data together with stage III SN Ia and BAO data (solid contours) and finally a Fisher matrix treatment of all data (dashed contours) as described further in the text.

ment. The Planck Fisher matrix was obtained from the Planck covariance matrix of  $(R, l_a, \Omega_b h^2, n_s)$ , with the appropriate parameter transformations for compatibility with the SN Ia and BAO Fisher matrices. See Appendix B for a description of how the Planck Fisher matrix was obtained and Table IV for the resulting Planck Fisher matrix. Constraints on dark energy parameters obtained in this way are also shown in Fig.3. Because of the nearly unconstrained directions, the pure Planck Fisher matrix cannot be inverted, as the range of eigenvalues is larger than its precision. This can be rectified with weak priors on the parameters (in which case diagonal entries in the inverse of the Fisher matrix will reflect those priors), or by adding more data. Figure 3 shows that the Fisher matrix is valid in spite of its formal problems: the error contours for Planck + SN-Ia + BAO data agree very well with the others.

## V. CONCLUSIONS

We have found that a Gaussian likelihood based on  $R$ ,  $l_a$ ,  $\Omega_b h^2$  and  $n_s$  effectively summarizes the information in Planck that is relevant for an analyses of data from SN Ia and BAO experiments for dark energy parameters under different dark energy models. Therefore a Planck prior can be included in this manner. When used in conjunction with other data that are more sensitive to dark energy such a treatment of Planck data results in no information loss as compared to a full analysis, while being much faster.

We provide the full  $R$ ,  $l_a$ ,  $\Omega_b h^2$ ,  $n_s$  covariance matrix that is required to define such a likelihood from Planck. We also provide a Planck Fisher matrix for people who prefer to use the Fisher matrix route to forecasting constraints for a future experiment. Using such a Planck prior we have obtained the type of constraints that may be expected from a stage III SN Ia and BAO survey. Of course the prescription can also be used once data from all these experiments have actually been obtained (ie. the prescription is not just for forecasting).

In the above analysis we found that it was not strictly necessary to include  $n_s$  given our conservative treatment of BAO data. A fuller treatment of BAO data such as one that included the shape of the matter power spectrum rather than the transverse and line of sight distances to the redshifts of the BAO survey deduced from the BAO scales in the corresponding directions, would require the primordial power spectrum parameters including  $n_s$  to be considered a variable in the BAO part of the analysis. For this reason we have included  $n_s$  in our prescription, and marginalized over it in our results.

While this work was in progress [28] considered a likelihood analysis involving the locations of the peaks and troughs in the CMB spectrum observed by WMAP to constrain dark energy parameters in combination with recent BAO data. This offers another way to include information from the CMB in a likelihood analysis of

BAO and SN Ia data. It involves fitting formulae for the locations of the extrema presented in [29]. Fitting formulae have been derived to account for certain pre-recombination effects that via the early ISW effect can effect the position of the first peak relative to the higher peaks. In our formalism we would have to recompute the  $R$ ,  $l_a$ ,  $\Omega_b h^2$  and  $n_s$  constraints for each new pre-recombination scenario, such as involving a non-zero neutrino mass, involving tensors and/or the running of the scalar spectral index, or else include these parameters in the covariance matrix. On the other hand, our approach is arguably simpler to implement, and at least as accurate within its domain of applicability (since it additionally uses  $R$  as an effective measure of peak height). In their approach too new fitting formulae would have to be derived new effects in different scenarios that haven't been considered in the past.

### Acknowledgements

We thank Pier-Stefano Corasaniti and Julien Larena for interesting discussions. MK acknowledges partial funding by the Swiss NSF. PM acknowledges the Department of Physics and Astronomy, University of Sussex, for support.

### APPENDIX A: DETAILED DESCRIPTION AND FORMULAE

The Planck satellite will deliver data of such a high quality that even small changes in parameters like the CMB temperature can have a significant impact. For this reason we summarise here the relevant formulae used in this paper. Generally they are those used by CAMB.

The comoving distance to a redshift  $z$  is given by

$$r(z) = cH_0^{-1} |\Omega_k|^{-1/2} \text{sinn}[|\Omega_k|^{1/2} \Gamma(z)] \quad (\text{A1})$$

$$\Gamma(z) = \int_0^z \frac{dz'}{E(z')}, \quad E(z) = H(z)/H_0$$

where  $\Omega_k = -k/H_0^2$  with  $k$  denoting the curvature constant, and  $\text{sinn}(x) = \sin(x)$ ,  $x$ ,  $\sinh(x)$  for  $\Omega_k < 0$ ,  $\Omega_k = 0$ , and  $\Omega_k > 0$  respectively, and

$$E(z) = [\Omega_m(1+z)^3 + \Omega_{\text{rad}}(1+z)^4] \quad (\text{A2})$$

$$+ \Omega_k(1+z)^2 + \Omega_X X(z)]^{1/2} \quad (\text{A3})$$

with  $\Omega_X = 1 - \Omega_m - \Omega_{\text{rad}} - \Omega_k$ , and the dark energy density function  $X(z) \equiv \rho_X(z)/\rho_X(0)$ .

We calculate the distance to decoupling,  $z_{CMB}$ , via the fitting formula in [22]. CAMB [23] uses the same fitting formula. We note that simply using a constant for  $z_{CMB}$  results in a shift in the inferred values of the CMB shift parameters at levels of precision corresponding to Planck. The comoving sound horizon at recombination

is given by

$$\begin{aligned} r_s(z_{CMB}) &= \int_0^{t_{CMB}} \frac{c_s dt}{a} = cH_0^{-1} \int_{z_{CMB}}^{\infty} dz \frac{c_s}{E(z)}, \\ &= cH_0^{-1} \int_0^{a_{CMB}} \frac{da}{\sqrt{3(1 + \bar{R}_b a) a^4 E^2(z)}} \quad (\text{A4}) \end{aligned}$$

where  $a$  is the cosmic scale factor,  $a_{CMB} = 1/(1 + z_{CMB})$ , and  $a^4 E^2(z) = \Omega_{\text{rad}} + \Omega_m a + \Omega_k a^2 + \Omega_X X(z) a^4$ . The radiation density is computed using the Stefan-Boltzmann formula from the CMB temperature, assuming 3.04 families of massless neutrini. The sound speed is  $c_s = 1/\sqrt{3(1 + \bar{R}_b a)}$ , with  $\bar{R}_b a = 3\rho_b/(4\rho_\gamma)$ ,  $\bar{R}_b = 31500\Omega_b h^2 (T_{CMB}/2.7 \text{ K})^{-4}$ .<sup>2</sup>

### APPENDIX B: FISHER MATRIX APPROACH

The Fisher matrix,  $F_{\alpha\beta}$ , for a set of parameters  $\mathbf{p}$  can be derived from the Fisher matrix,  $F_{ij}$ , for a set of equivalent parameters  $\mathbf{q}$  as follows [20]

$$F_{\alpha\beta} = \sum_{ij} \frac{\partial p_i}{\partial q_\alpha} F_{ij} \frac{\partial p_j}{\partial q_\beta}. \quad (\text{B1})$$

The Fisher matrix of  $\mathbf{q} = (R, l_a, \omega_b, n_S)$  is the inverse of the covariance matrix of  $\mathbf{q}$  (given in Tables I and II). Note that the CMB shift parameters  $R$  and  $l_a$  encode all the information on dark energy parameters. For any given dark energy model parameterized by the parameter set  $\mathbf{p}_X$ , the relevant Fisher matrix for  $\mathbf{p} = (\mathbf{p}_X, \Omega_{DE}, \Omega_k, \omega_m, \omega_b, n_S)$  can be found using Eq.(B1). For the case most discussed in the literature,  $w_X(z) = w_0 + w_a(1-a)$ ,  $\mathbf{p}_X = (w_0, w_a)$ .

In order to find the Fisher matrix for  $(w_0, w_a, \Omega_{DE})$ ,

<sup>2</sup> We used a  $T_{CMB} = 2.726$ , and  $\bar{R}_b = 30000\Omega_b h^2$  as defined in CAMB, noting that precision can be improved by updating these definitions.

$\Omega_k, \omega_m, \omega_b, n_S$ ), the following derivatives are needed:

$$\begin{aligned}
\frac{\partial R}{\partial w_i} &= \frac{\partial \Gamma(z_{CMB})}{\partial w_i} \sqrt{\Omega_m} \text{cosn} \left[ |\Omega_k|^{1/2} \Gamma(z_{CMB}) \right] \\
\frac{\partial \ln R}{\partial \Omega_{DE}} &= -\frac{1}{2\Omega_m} + |\Omega_k|^{1/2} \\
&\quad \frac{\text{cosn} \left[ |\Omega_k|^{1/2} \Gamma(z_{CMB}) \right]}{\text{sinn} \left[ |\Omega_k|^{1/2} \Gamma(z_{CMB}) \right]} \frac{\partial \Gamma(z_{CMB})}{\partial \Omega_{DE}} \\
\frac{\partial \ln R}{\partial \Omega_k} &= -\frac{1}{2\Omega_m} - \frac{1}{2\Omega_k} + |\Omega_k|^{1/2} \\
&\quad \frac{\text{cosn} \left[ |\Omega_k|^{1/2} \Gamma(z_{CMB}) \right]}{\text{sinn} \left[ |\Omega_k|^{1/2} \Gamma(z_{CMB}) \right]} \left[ \frac{\partial \Gamma(z_{CMB})}{\partial \Omega_k} + \frac{\Gamma(z_{CMB})}{2\Omega_k} \right] \\
\frac{\partial R}{\partial \omega_m} &= 0, \quad \frac{\partial R}{\partial \omega_b} = 0, \quad \frac{\partial R}{\partial n_S} = 0 \\
\frac{\partial \ln l_a}{\partial w_i} &= |\Omega_k|^{1/2} \frac{\text{cosn} \left[ |\Omega_k|^{1/2} \Gamma(z_{CMB}) \right]}{\text{sinn} \left[ |\Omega_k|^{1/2} \Gamma(z_{CMB}) \right]} \\
&\quad \frac{\partial \Gamma(z_{CMB})}{\partial w_i} - \frac{\partial \ln[H_0 r_s(z_{CMB})]}{\partial w_i} \\
\frac{\partial \ln l_a}{\partial \Omega_{DE}} &= |\Omega_k|^{1/2} \frac{\text{cosn} \left[ |\Omega_k|^{1/2} \Gamma(z_{CMB}) \right]}{\text{sinn} \left[ |\Omega_k|^{1/2} \Gamma(z_{CMB}) \right]} \\
&\quad \frac{\partial \Gamma(z_{CMB})}{\partial \Omega_{DE}} - \frac{\partial \ln[H_0 r_s(z_{CMB})]}{\partial \Omega_{DE}} \\
\frac{\partial \ln l_a}{\partial \Omega_k} &= -\frac{1}{2\Omega_k} + |\Omega_k|^{1/2} \frac{\text{cosn} \left[ |\Omega_k|^{1/2} \Gamma(z_{CMB}) \right]}{\text{sinn} \left[ |\Omega_k|^{1/2} \Gamma(z_{CMB}) \right]} \\
&\quad \left[ \frac{\partial \Gamma(z_{CMB})}{\partial \Omega_k} + \frac{\Gamma(z_{CMB})}{2\Omega_k} \right] - \frac{\partial \ln[H_0 r_s(z_{CMB})]}{\partial \Omega_k} \\
\frac{\partial \ln l_a}{\partial \omega_m} &= -\frac{\partial \ln[H_0 r_s(z_{CMB})]}{\partial \omega_m}, \\
\frac{\partial \ln l_a}{\partial \omega_b} &= -\frac{\partial \ln[H_0 r_s(z_{CMB})]}{\partial \omega_b}, \\
\frac{\partial l_a}{\partial n_S} &= 0 \\
\frac{\partial \omega_b}{\partial \omega_b} &= 1, \quad \frac{\partial \omega_b}{\partial p_i} = 0 \quad (p_i \neq \omega_b) \\
\frac{\partial n_S}{\partial n_S} &= 1, \quad \frac{\partial n_S}{\partial p_i} = 0 \quad (p_i \neq n_S), \tag{B2}
\end{aligned}$$

where  $w_i = (w_0, w_a)$ , and  $\text{cosn}(x) = \cos(x)$ ,  $x$ ,  $\text{cosh}(x)$  for  $\Omega_k < 0$ ,  $\Omega_k = 0$ , and  $\Omega_k > 0$  respectively.

Note that in the limit of  $\Omega_k = 0$ ,

$$\begin{aligned}
\frac{\partial \ln R}{\partial \Omega_k} &= \frac{\partial \ln \Gamma(z_{CMB})}{\partial \Omega_k} - \frac{1}{2\Omega_m} + \frac{[\Gamma(z_{CMB})]^2}{6} \\
\frac{\partial \ln l_a}{\partial \Omega_k} &= \frac{\partial \ln \Gamma(z_{CMB})}{\partial \Omega_k} - \frac{\partial \ln[H_0 r_s(z_{CMB})]}{\partial \Omega_k} + \\
&\quad \frac{[\Gamma(z_{CMB})]^2}{6} \tag{B3}
\end{aligned}$$

For the fiducial model considered in this paper, the Planck Fisher matrix for  $(w_0, w_a, \Omega_{DE}, \Omega_k, \omega_m, \omega_b, n_S)$  is derived from the Planck covariance matrix of  $(R, l_a, \omega_b, n_S)$  given in Table IV.

## APPENDIX C: USING OUR LIKELIHOOD FOR HAMILTONIAN MONTE CARLO

While most cosmological codes use the standard Metropolis MCMC algorithm, there are other MC approaches which may provide faster exploration especially in high dimensions. One example is Hamiltonian Monte Carlo (HMC) [31, 32] where each parameter  $\theta_i$  acquires a partner corresponding to a momentum variable  $\pi_i$ , and the log-likelihood is regarded as a potential. The momenta are drawn from a univariate normal probability distribution and the next step in the MCMC exploration is chosen based on a Hamiltonian motion in this system, with total energy  $E = p^2/2 + \chi^2(\theta)/2$ . At the end the momenta are marginalised over, which provides an ensemble of samples of the remaining parameters which is drawn from the posterior distribution. The main advantage of the HMC method is that the Hamiltonian motion naturally follows even complicated shapes of the posterior and in principle every proposal is accepted. The main drawback is that, in order to follow the trajectory, one needs to evaluate the gradient of the log-likelihood with respect to the parameters for dozens of steps, for every single proposal. Each proposal therefore requires hundred(s) of likelihood evaluations if the gradient cannot be computed analytically.

Since we have a reasonable approximation of the likelihood, we can instead use this approximation to compute the gradients. This means that the motion follows the  $(R, l_a, \omega_b, n_S)$  likelihood and at the end the approximate and the true likelihood are compared. If the true likelihood is worse than the approximate one, then we can either assign the ratio as a weight to the new point (importance sampling) or test for rejection with the usual criterion (rejection sampling). If the true likelihood is better, then have to assign the ratio as a weight  $> 1$ . For this to work we must ensure that the approximate likelihood does not exclude parameter regions that the true likelihood would allow.

In our case we find that the procedure works quite well for the case where the Planck data is combined with the SN Ia and BAO data, since there the information loss is negligible<sup>3</sup>. Indeed, we find about 20% efficiency (ie roughly every 5th proposal is accepted, or correspondingly, the average weight of each point is 0.2), which is very good, especially since we can move a long distance and obtain completely uncorrelated samples. Using only the Planck data, we lose a lot of information, and less than 2% of the proposals are accepted. This is still not too bad, considering the complexity of the shape of the posterior, and that the resulting samples are completely decorrelated. Additionally, burn-in is very quick

<sup>3</sup> We add additionally  $\tau$  and  $\ln A_s$  to the set of our parameters, and augment the  $(R, l_a, \omega_b, n_S)$  likelihood with their 2x2 covariance matrix.

for HMC and there is no need for initial runs to determine the optimal proposal matrix.

- 
- [1] Kunz, M., Sapone, D, 2007, *Phys.Rev.Lett.*, 98, 121301
- [2] Carroll, S M, de Felice, A, Duvvuri, V, Easson, D A, Trodden, M & Turner, M S, *Phys.Rev. D* 71 (2005) 063513
- [3] Onemli, V. K., & Woodard, R. P. 2004, *Phys.Rev. D* 70, 107301
- [4] Cardone, V.F., Tortora, C., Troisi, A., & Capozziello, S. 2005, *astro-ph/0511528*, *Phys.Rev.D*, in press
- [5] Kolb, E.W., Matarrese, S., & Riotto, A. 2005, *astro-ph/0506534*
- [6] Caldwell, R.R.; Komp, W.; Parker, L.; Vanzella, D.A.T., *Phys.Rev. D* 73 (2006) 023513
- [7] E. O. Kahya and V. K. Onemli, *gr-qc/0612026*
- [8] de Felice, A., Mukherjee, P., & Wang, P., 2007, *PRD* in press, *astro-ph/0706.1197*
- [9] Koivisto, T.; Mota, D.F., *hep-th/0609155*, *Phys.Rev. D* 75 (2007) 023518
- [10] Ng, Y.J., *gr-qc/0703096*
- [11] A. R. Liddle, P. Mukherjee, D. Parkinson and Y. Wang, 2006, *Phys. Rev. D* **74** 123506 [*arXiv:astro-ph/0610126*].
- [12] Albrecht, A.; Bernstein, G.; Cahn, R.; Freedman, W. L.; Hewitt, J.; Hu, W.; Huth, J.; Kamionkowski, M.; Kolb, E.W.; Knox, L.; Mather, J.C.; Staggs, S.; Suntzeff, N.B., Report of the Dark Energy Task Force, *astro-ph/0609591*
- [13] Spergel, D.N., et al. 2006, *astro-ph/0603449*, *ApJ*, in press
- [14] Y. Wang and P. Mukherjee, 2007, *PRD* in press, *arXiv:astro-ph/0703780*.
- [15] Y. Wang and P. Mukherjee, 2006, *Astrophys. J.* **650**, 1
- [16] Y. Wang and P. Mukherjee, 2004, *Astrophys. J.* **606**, 654
- [17] C. Pahud, A. R. Liddle, P. Mukherjee and D. Parkinson, *Phys. Rev. D* **73** (2006) 123524 [*arXiv:astro-ph/0605004*]
- [18] Blake, C., Parkinson, D., Bassett, B., Glazebrook, K., Kunz, M. and Nichol, R.C., 2006, *Mon. Not. Roy. Astron. Soc.* **365**, 255
- [19] Seo, H. J. and Eisenstein, D. J., 2003, *Astrophys. J.* **598** 720
- [20] Wang, Y., 2006, *ApJ*, 647, 1
- [21] A. Lewis and S. Bridle, *Phys. Rev. D* **66** (2002) 103511 [*arXiv:astro-ph/0205436*].
- [22] Hu, W., & Sugiyama, N., 1996, *Astrophys.J.* 471, 542-570
- [23] Lewis, A., Challinor, A., Lasenby, A., 2000, *Astrophys. J.*, 538, 473-476
- [24] Chevallier, M., & Polarski, D. 2001, *Int. J. Mod. Phys. D* 10, 213
- [25] Corasaniti, P.S., Kunz, M., Parkinson, D., Copeland E.J. and Bassett, B.A., *Phys.Rev. D* 70 (2004) 083006
- [26] Eisenstein, D., et al., *ApJ*, 633, 560
- [27] Some WFMOS paper (our optimisation I?)
- [28] Corasaniti, P.S. and Melchiorri, A., 2007, *arXiv:0711.4119* [*astro-ph*]
- [29] Doran, M. and Lilley, M., 2002, *Mon. Not. Roy. Astron. Soc.* **330** 965 [*arXiv:astro-ph/0104486*]
- [30] M. Kunz, *arXiv:astro-ph/0702615* (2007).
- [31] D.J.C. MacKay, *Information theory, Inference, and Learning Algorithms*, Cambridge University Press (2003).
- [32] A. Hajian, *Phys. Rev. D* 75, 083525 (2007) .

TABLE I:  $R$ ,  $l_a$ ,  $\Omega_b h^2$  and  $n_s$  estimated from Planck simulated data.

| Parameter         | mean    | rms     | variance |
|-------------------|---------|---------|----------|
| $\Omega_k \neq 0$ |         |         |          |
| $R$               | 1.7016  | 0.0055  |          |
| $l_a$             | 302.108 | 0.098   |          |
| $\Omega_b h^2$    | 0.02199 | 0.00017 |          |
| $n_s$             | 0.9602  | 0.0038  |          |

TABLE II: Covariance matrix for  $(R, l_a, \Omega_b h^2, n_s)$  from Planck.

|                   | $R$           | $l_a$         | $\Omega_b h^2$ | $n_s$         |
|-------------------|---------------|---------------|----------------|---------------|
| $\Omega_k \neq 0$ |               |               |                |               |
| $R$               | 0.303492E-04  | 0.297688E-03  | -0.545532E-06  | -0.175976E-04 |
| $l_a$             | 0.297688E-03  | 0.951881E-02  | -0.759752E-05  | -0.183814E-03 |
| $\Omega_b h^2$    | -0.545532E-06 | -0.759752E-05 | 0.279464E-07   | 0.238882E-06  |
| $n_s$             | -0.175976E-04 | -0.183814E-03 | 0.238882E-06   | 0.147219E-04  |

TABLE III: Normalized covariance matrix for  $(R, l_a, \Omega_b h^2, n_s)$  from Planck.

|                   | $R$       | $l_a$     | $\Omega_b h^2$ | $n_s$     |
|-------------------|-----------|-----------|----------------|-----------|
| $\Omega_k \neq 0$ |           |           |                |           |
| $R$               | 1.        | 0.553856  | -0.592359      | -0.832527 |
| $l_a$             | 0.553856  | 1.        | -0.465820      | -0.491026 |
| $\Omega_b h^2$    | -0.592359 | -0.465820 | 1.             | 0.372425  |
| $n_s$             | -0.832527 | -0.491026 | 0.372425       | 1.        |

TABLE IV: Fisher matrix for  $(w_0, w_a, \Omega_{DE}, \Omega_k, \omega_m, \omega_b, n_S)$  derived from the covariance matrix for  $(R, l_a, \Omega_b h^2, n_s)$  from Planck.

|               | $w_0$        | $w_a$        | $\Omega_{DE}$ | $\Omega_k$   | $\omega_m$   | $\omega_b$   | $n_S$        |
|---------------|--------------|--------------|---------------|--------------|--------------|--------------|--------------|
| $w_0$         | .172276E+06  | .490320E+05  | .674392E+06   | -.208974E+07 | .325219E+07  | -.790504E+07 | -.549427E+05 |
| $w_a$         | .490320E+05  | .139551E+05  | .191940E+06   | -.594767E+06 | .925615E+06  | -.224987E+07 | -.156374E+05 |
| $\Omega_{DE}$ | .674392E+06  | .191940E+06  | .263997E+07   | -.818048E+07 | .127310E+08  | -.309450E+08 | -.215078E+06 |
| $\Omega_k$    | -.208974E+07 | -.594767E+06 | -.818048E+07  | .253489E+08  | -.394501E+08 | .958892E+08  | .666335E+06  |
| $\omega_m$    | .325219E+07  | .925615E+06  | .127310E+08   | -.394501E+08 | .633564E+08  | -.147973E+09 | -.501247E+06 |
| $\omega_b$    | -.790504E+07 | -.224987E+07 | -.309450E+08  | .958892E+08  | -.147973E+09 | .405079E+09  | .219009E+07  |
| $n_S$         | -.549427E+05 | -.156374E+05 | -.215078E+06  | .666335E+06  | -.501247E+06 | .219009E+07  | .242767E+06  |